Research
Volume 10:8, 2021

Journal of Material Sciences & Engineering

ISSN: 2169-0022

Open Access

Developing a Practical Chemical Process to Prepare Boron-Doped Carbon (CB_x) Materials with High Thermal-Oxidative Stability

Joseph Vandy Sengeh, Wei Zhu, Houxiang Li and T. C. Mike Chung*

Department of Materials Science and Engineering, The Pennsylvania State University, USA

Abstract

This paper discusses a new method to prepare boron doped carbon (CB_x) material with some substitutional boron atoms homogeneously distributed in the highly graphitic structure. The chemistry involves a mesophase boron-doped pitch (B-Pitch) prepared by mixing a borane reagent (i.e., dichlorophenylacetylborane) with petroleum pitch at 400°C. The resulting mesophase B-Pitch was further diluted with the starting pitch to adjust its softening temperature and melt viscosity, they are essential during the preparation of C/C composites. A resulting B-Pitch/Pitch blended precursor with 3.3 mol% B content and a softening temperature of 300°C was directly converted to CB_x at 2300°C under argon atmosphere, showing a char yield of 81%. The presence of a small percentage of B atoms in this B-Pitch/Pitch precursor catalyzes the carbonization/graphitization to form a highly graphitic CB_x structure. Compared to synthetic graphite, which is stable in air up to 500°C, the resulting CB_x shows higher thermal-oxidative stability. In air at 600°C, no weight loss was observed after 6 hours. At 700°C and 800°C, there was no detectable weight loss for 80 minutes. Evidently, the homogeneous distribution of B atoms in the CB_x matrix is essential in continuously providing a protective B_2O_3 surface layer to slow down the oxygen diffusion into the matrix and delay the thermal/oxidative degradation process. Overall, this new precursor technology may offer the C/C composite manufacturing with reduced pyrolysis cycles and increased thermal/oxidative stability in high temperature applications.

Keywords: Boron-doped carbon • Petroleum pitch • Boron-doped pitch • Char yield • Thermal-oxidative stability

Introduction

Carbon (C) materials, including C/C composites and graphite, are known to begin significant thermal-oxidative decomposition in air when the temperature reaches ~500°C [1,2]. It has long been of scientific interest and technological importance to improve the thermal-oxidative stability and expand the applications of these materials to higher temperatures [3-12]. Due to the difficulties in the chemical modification of graphitic C structures, most approaches are based on surface coating or surface functionalization to provide a protective layer, which slows oxygen diffusion into C materials [13-17]. In addition to a thin surface protection layer, the combination of thermal expansion and weak interface adhesion often limits the effectiveness of the protective layer for long-term applications [18-20].

Boron (B) has an atomic size similar to that of the C atom and forms a covalent B-C bond; it is the only element known to substitute into the graphene layer, with a maximum level of ~2 mol% [21-23]. The electron-deficient (acidic) B atoms present in the π-electron conjugated graphene layer can induce p-type doping to reduce the overall oxidation potential. Thus, B-doping has the potential to intrinsically increase the oxidative stability of the carbon material [24-27]. Jones et al. showed that a boron concentration at all levels of the C material can inhibit its thermal-oxidative activity [21]. Most B-modified C materials have been prepared by post carbonization processes, which involve surface modification or coating of the preformed C materials. Several boron compounds, including boric acid, ethyl borates, boron oxide, and elemental boron, are commonly used as reagents in chemical vapor deposition (CVD) and reactive mixing to alter the surface structures and properties of carbon materials and C/C composites [28-32]. In this approach, a high temperature (>2000°C) is required to incorporate boron into the graphene structure. In addition to high energy requirements, the diffusion of boron into the highly crystalline matrix is difficult, as it typically results in a concentrated B distribution on the surfaces of C materials. Using a different approach, Howe et al. carried out the reactive mixing of PAN precursor fibers with amorphous boron powder at high temperatures between 1700°C and 2487°C [33]. They observed the presence of B-doping in the resulting carbon fiber (CF). In addition to improving the CF thermal-oxidative stability, the presence of boron also helps the graphitization reaction occur at lower temperatures. Zhai et al. showed a similar B-catalyzed graphitization phenomenon with the transformation of amorphous carbon into highly crystalline graphite [34].

Approximately a decade ago, Hu et al. in our group reported an organo-boron compound (9-chloroborafluorene) that shows effective thermal transformation to a boron-doped carbon structure under an inert atmosphere [35]. The concentration of B incorporated into the resulting material was dependent on the pyrolysis temperature and the associated crystalline structure. There is a significant downside of the 9-chloroborafluorene precursor that is difficult to prepare with a low yield and high cost. This paper did not investigate the melt processability of the precursor and the thermal-oxidative properties of the resulting materials. In this paper, we will discuss a practical method to prepare boron-doped carbon products involving low-cost petroleum pitch and the thermal-oxidative stability of the resulting B-doped carbon (CB_x) products.

***Address for Correspondence:** TC Mike Chung, Department of Materials Science and Engineering, The Pennsylvania State University, USA, Email: tcc3@psu.edu*

Received: 06 August, 2021; **Accepted**: 20 August, 2021; **Published**: 27 August, 2021

Materials and Instrumentation

Boron trichloride and 1-phenyl-2-trimethylsilylacetylene were purchased from Sigma Aldrich and used as received. They were handled in a dry box under argon atmosphere. Isotropic petroleum pitch was obtained from RÜTGERS Germany GmbH.

All solution ^1H NMR, ^{13}C NMR, and ^{11}B NMR spectra were recorded on a Bruker Nanobay-400 MHz spectrometer equipped with an iprobe (400 MHz for ^1H, 100 MHz for ^{13}C, and 160 MHz for ^{11}B). Solid-state ^{11}B NMR spectra were recorded using Avance-III-HD ss-500 to determine the boron content and chemical shift of the B-pitch precursors. A polarized optical microscope (Olympus) was used to examine the optically anisotropic structure of the samples. The sample was placed in an abrasive, and epoxy resin and curing agent were added. After curing, the samples were polished with different grits (320-1200 μm) of sandpaper to a flat and smooth surface and examined under a microscope. MALDI-TOF MS spectra were measured using a Bruker Ultraflextreme matrix-assisted laser desorption ionization time-of-flight tandem mass spectrometer equipped with a 1 kHz smart beam-II laser. The precursor rheological properties were investigated using an ARES-G2 rotational rheometer (TA Instruments, New Castle, DE) equipped with 8 mm parallel plates. Controlled strain measurements were taken under an inert environment (nitrogen). A temperature sweep from 250°C to 400°C was performed on the samples at a shear rate of 0.1 rad/sec with a 10% strain rate. A frequency sweep experiment was performed under similar conditions at two different temperatures (310°C and 360°C). Thermogravimetric (TGA) analysis was performed on a TA 600 instrument from 50°C−1000°C at a heating rate of 10°C/min in a nitrogen atmosphere. Thermomechanical (TMA) analysis to determine the softening point of the precursors was performed using a TA 450 instrument from 50°C−400°C at a heating rate of 10°C /min in an inert environment.

Synthesis of dichlorophenylacetylborane

In a dry box, boron trichloride (52.5 mL, 60 mM) in 1 M dichloromethane solution was injected into a 100 mL round bottom flask before slowly adding 1-phenyl-2-trimethylsilylacetylene (10 mL, 51 mM) over a period of 5-10 minutes. The mixed solution was stirred at room temperature, with a color change from light yellow to dark brown within 10 minutes. After 3 hours, the reaction was stopped, and the flask was removed from the glovebox and connected to a Schlenk line under N_2 atmosphere. The subsequent distillation was carried out at 60°C to remove trimethylsilyl chloride byproduct and some unreacted boron trichloride. Dichlorophenylacetylborane product (8.6 g dark brown liquid with 93.5% yield) was then isolated and used for the subsequent reaction. The following data were obtained: ^1H NMR spectrum: δ 6.8, 6.9, 7.05 ppm; 13C NMR spectrum: δ 113.3, 119.6, 126.8, 129.8, and 131.6 ppm; 11B NMR spectrum: δ 42.9 ppm (sharp, high intensity peak) and 39.55 ppm (lower peak intensity). The spectra (Figures S1-S3) are included in the Supplementary Information.

Synthesis of B-pitch/pitch blended precursor

In a typical reaction, the resulting dichlorophenylacetylborane reagent was mixed with isotropic petroleum pitch (at a 1/1 weight ratio) under an inert gas atmosphere. After heating the mixture at 400°C for 24 hours under a pressurized system with mild agitation, a cycloaddition reaction occurred to form B-Pitch with 86% mesophase, as measured by polarized optical microscopy. The resulting mesophase B-Pitch was then blended with the starting isotropic pitch at 310°C (with the weight ratio shown in Table 1) to form the melt-processible B-Pitch/Pitch mixed precursor. This melt blending procedure was performed in a plastic corder PL 2000 twin-screw Brablender with a spinning rate of 200 rpm and flow rate of 100 ml/min.

Thermal conversion of B-pitch/pitch blended precursor to CB_x materials

The B-Pitch/Pitch blended precursors were carbonized at higher temperatures using a graphite resistance-type furnace manufactured by Centorr Vacuum Technology. The furnace was evacuated to a vacuum of 150 mTorr and then pressurized to 2 psi with ultrahigh purity argon. This process was repeated twice thereafter to ensure the elimination of air from the furnace before heating to higher temperatures. The heating rate of the furnace was 15°C/min, which was controlled manually. A thermocouple and optical pyrometer were used to monitor the temperature of the furnace.

Characterization of CB_x materials

The boron elemental composition in the CB_x products was analyzed using the thermo ICAP 7400 inductively coupled plasma emission spectrum (ICP). Boron concentration was determined at a wavelength of 249.77 nm. Synthetic, high-purity standards were used to calibrate the results. The detection limit of this technique is reported to be ~0.01 ppm. Raman spectra were obtained using the Horiba LabRam HR Evolution Vis-NIR optimized and the AIST-NT Scanning Probe instrument. Raman excitation was performed at room temperature using 532 nm lasers light with a typical incident laser power of 10%. The accumulation time was approximately 2 min. X-ray diffraction measurements were made on a Malvern Panalytical X'Pert Pro MPD theta-theta diffractometer. The instrument employed Cu Kα radiation operating at 40 mA and 45 kV. Finely ground CB_x powder samples were used. Measurements were made from 10°C to 80°C, and the d-spacing and crystal height were calculated from the (002) reflection peak.

X-ray photoelectron spectroscopy (XPS) was performed using a Physical Electronics VersaProbe II instrument equipped with a monochromatic Al Kα X-ray (1,486.7 eV) source and a concentric hemispherical analyzer. Charge neutralization was performed using both low-energy electrons (<5 eV) and argon ions. The binding energy axis was calibrated using sputter-cleaned Cu (Cu $2p_{3/2}$=932.62 eV, Cu $3p_{3/2}$=75.1 eV) and Au foils (Au $4f_{7/2}$=83.96 eV). Peaks referenced the CH_x band in the carbon 1 s 1s spectra at 284.8 eV. Measurements were made at a take-off angle of 45º with respect to the sample surface plane. This resulted in a typical sampling depth of 3-6 nm (95% of the signal originated from this depth or shallower). Quantification was performed using instrumental relative sensitivity factors (RSFs) that account for the X-ray cross section and inelastic mean free path of the electrons

Results and Discussion

As discussed, this research involves three closely related objectives: (i) the preparation of melt-processable B-Pitch/Pitch precursors, (ii) thermal transformation of the resulting precursors to the corresponding boron-doped carbon (CB_x) materials with high residue yield and highly graphitic structure, and (iii) the evaluation of the thermal-oxidative stability of the resulting CB_x materials at high temperatures in air.

Synthesis and melt-processing of B-pitch/pitch blended precursor

Figure 1 shows a facile blending process to prepare the melt-processible B-Pitch/Pitch blended precursors, which involves two consecutive blending steps under specific temperatures and N_2 atmosphere. The first step is reactive blending between petroleum pitch (I) and a borane reagent (II), i.e., dichlorophenylacetylborane (DPB) at 400°C under a N_2 atmosphere. The preparation of the DPB reagent involves 1-phenyl-2-trimethylsilylacetylene and BCl_3, following the experimental procedure discussed in a previous paper [36]. Under homogeneous melt-blending conditions, a mixture of polycyclic aromatic hydrocarbon (PAH) molecules (enophiles) in petroleum pitch is combined with the DPB borane reagent (dienophile), and thermally induced (2+4) cycloaddition takes place to form the liquid-crystalline B-Pitch material with extended polycyclic aromatic structures, 86% mesophase morphology, and a high softening temperature (>400°C). In the consecutive blending step, in order to reduce the softening temperature and a suitable melt viscosity, the resulting mesophase B-Pitch material is homogeneously mixed (diluted) with a selected quantity of the starting petroleum pitch at 310°C (without any detectable chemical reaction) to obtain the desirable

B-Pitch/Pitch blended precursor that shows a suitable softening temperature and good melt processibility.

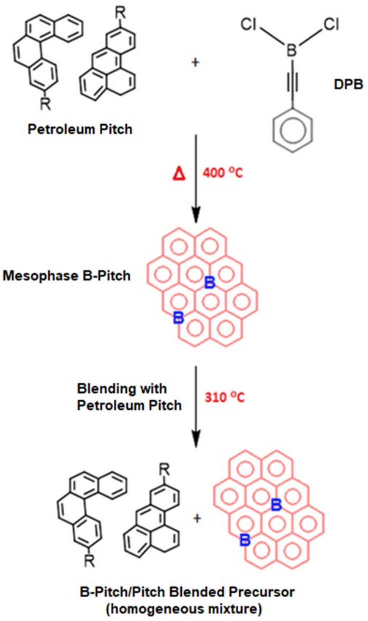

Figure 1. Two-step blending procedures for the fabrication of melt-processible B-Pitch/Pitch precursor

Figure 2 (top) compares two ^{11}B NMR spectra between the starting DPB reagent and the resulting mesophase B-Pitch material. Because of the limited solubility of the mesophase B-Pitch, this ^{11}B NMR measurement was conducted under solid-state conditions. The solution ^{11}B NMR spectrum of the DPB reagent shows a major sharp peak at 42 ppm, corresponding to the borane moiety in the DPB structure. There is a minor peak at 38 ppm, which is associated with the chlorodiphenylacetylborane structure formed after double substitution reactions of BCl_3 with two 1-phenyl-2-trimethylsilylacetylene reagents. After reactive melt-mixing at 400°C under a N_2 atmosphere, the ^{11}B chemical shifts move to high field in the range between 20 and -15 ppm. Evidently, the cycloaddition reaction occurs between DPB and PAH molecules in the pitch to form a new mesophase B-Pitch material with new B-substituted moieties, which are π-electrons conjugated with the extended polycyclic aromatic structure. The relatively broad chemical shift is partially due to the solid-state measurement with the quadrupolar nature of the boron nucleus [37], as well as various B moieties present in the B-Pitch material that are derived from a complex mixture of PAH molecules in the starting petroleum pitch [38-40]. As expected, some substitutional B atoms are located near the edge of the mesophase B-Pitch structure with less π-electron delocalization and lower chemical shifts. The mass increase of mesophase B-Pitch is also confirmed by MALDI-TOF measurement shown in Figure S4 of the Supplemental Information.

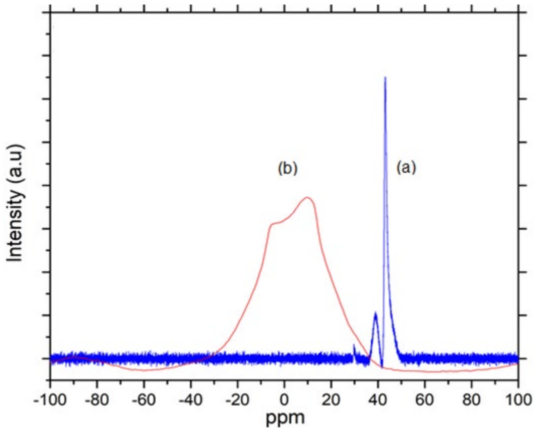

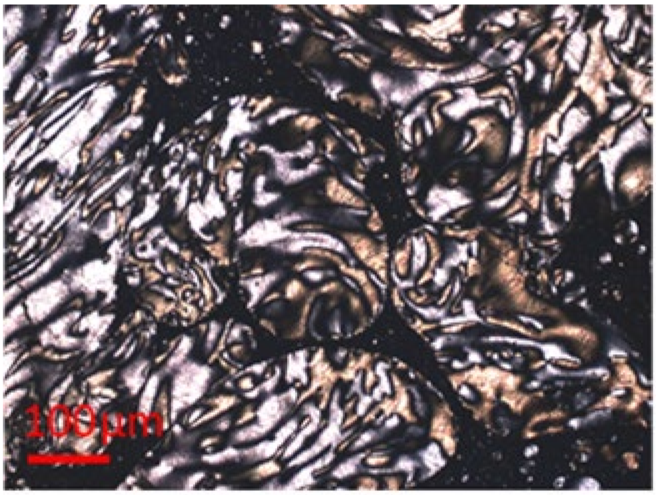

Figure 2. (top) ^{11}B NMR spectra of (a) the starting DPB reagent and (b) the resulting mesophase B-Pitch product and (bottom) shows the polarized optical micrograph of this B-Pitch material, which exhibits 86%mesophase morphology

To quantify the amount of boron atoms in the resulting mesophase B-Pitch material, a standard boric acid solution with known B content was also examined by ^{11}B NMR. The results were used as the external reference to estimate the B content in the sample by comparing peak intensities. As shown in Table 1, the resulting mesophase B-Pitch contains 4.7 mol% B atoms, implying a quantitative thermal-induced coupling reaction between DPB and various PAH molecules in pitch. Figure 2 (bottom) shows the polarized optical micrograph of this B-Pitch material, which exhibits 86% mesophase morphology. Overall, it has the appearance of Brooks and Taylor (BT) mesophase [41,42], in which there is complete local anisotropy while the material as a whole is statistically isotropic. As will be discussed later, this mesophase B-Pitch material is highly graphitizable with a high char yield (C-yield).

In addition to high C-yield, it is essential to prepare the melt-processible precursors for C/C composite and carbon fiber manufacturing [43-45]. The resulting mesophase B-Pitch material was then physically melt-blended (diluted) with the starting isotropic pitch using various weight ratios at 310°C to form B-Pitch/Pitch blended precursors. As shown in Table 1, with the increase in petroleum pitch (softening temperature at 167°C), which serves as plasticizer, the softening temperature of the resulting B-Pitch/Pitch blended precursor systematically reduced to the level that is typically applied in the melt processing of pitch precursors. The B content in the resulting B-Pitch precursor was also monitored by solid-state ^{11}B NMR spectra, as shown in Figure 3, with the peak intensity closely correlated to the expected boron content in the mixture. The identical chemical shift and shape between the starting mesophase B-Pitch and all B-Pitch/Pitch blended precursors also implies simple physical mixing without any

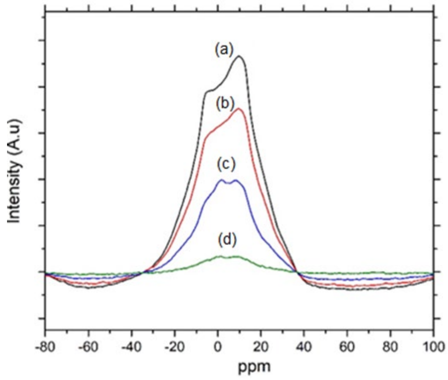

Figure 3. Solid-State ^{11}B NMR spectra of B-Pitch/Pitch blended precursors containing various weigh percentage of free isotropic petroleum pitch (a) 0%, (b) 30%, (c) 50%, and (d) 90%

Table 1. A summary of B-Pitch precursors with softening temperatures and C-yields

B-Pitch Precursor	B-Pitch/Pitch Weight Ratio	Boron Content* (wt.%)	Softening Temp. (ºC)	C-Yield (%)
Mesophase B-Pitch	100/0	4.7	>400	90
Precursor-1	80/20	3.7	>400	84
Precursor-2	75/25	3.5	>350	82
Precursor-3	70/30	3.3	300	81
Precursor-4	60/40	2.8	217	80
Precursor-5	50/50	2.0	190	75
Precursor-6	10/90	0.4	175	60
Petroleum Pitch	0/100	0	167	57

chemical reaction.

All four B-Pitch/Pitch blended precursors (with boron contents from 3.3 to 0.4 wt% in Table 1) appear to be melt processible based on the softening temperature. To understand the most suitable melt processing conditions, the samples were further subjected to rheological tests. Figure 4 (top) shows the temperature sweep of these B-Pitch/Pitch blended precursors with the plot of complex melt viscosity vs temperature under a constant oscillating frequency at 0.1 rad/sec. As expected, the melt viscosity of the B-Pitch/Pitch precursors decreases with increasing isotropic pitch content. The melt viscosity also follows that general trend, reducing the viscosity with increasing temperature. However, above 340°C, the melt viscosity becomes approximately constant or even increases slightly, which implies some molecular enlargement in the B-Pitch precursor structure. As shown in the Supplemental Information (Figure S5), matrix-assisted laser desorption/ionization (MALDI-TOF) spectroscopy was employed to confirm the increase in the size of the precursor molecules at 350°C. Since the common PAH molecules in pitch are chemically stable under this temperature condition, the increase in precursor size may be caused by the boron-catalyzed cycloaddition reaction between pitch molecules. However, the complex melt viscosity for the four precursors is still within the common melt-processing window in the range of 10^2-10^4 Pa-s [46-49].

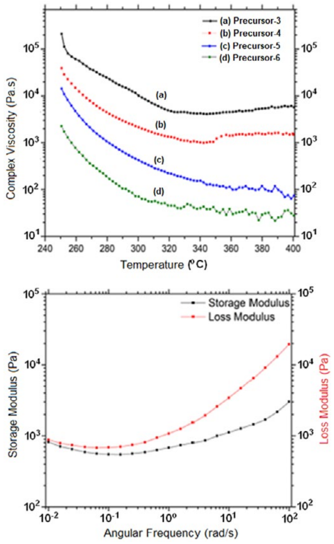

Figure 4. (Top) plot of complex viscosity vs temperature (with 0.1 rad/sec frequency) for (a) Precursor-3, (b) Precursor-4, (c) Precursor-5, and (d) Precursor-6, and (Bottom) frequency sweep of Precursor-3 with storage and loss modulus vs frequency plots at 310ºC

Based on the temperature sweep study, the minimum melt-processing temperature for Precursor-3 is ~310°C. Figure 4 (bottom) shows the frequency sweep for this precursor at 310 °C with plots of both storage modulus and loss modulus vs angular frequency. Under low-frequency shear (<0.1 rad/sec), in which the system has enough time to relax, both the storage modulus and loss modulus are relatively constant. With the increase in shear frequency to >0.1 rad/sec, both the storage modulus and the loss modulus increase as well, indicating slow relaxation. Across the whole frequency range, the loss modulus is always higher than the storage modulus (no crossover point), which implies viscoelastic properties. Two parallel experimental results at 260 and 360°C are presented in the Supplemental Information. The frequency sweep at 360°C shows a significant increase in both moduli (including the low shear range), which clearly indicates an increase in molecular mass due to coupling reactions between the mixed molecules. Evidently, all four B-Pitch/Pitch precursors are suitable for melt processing at various temperatures, and the B-Pitch/Pitch precursor with 30 wt.% free pitch (a plasticizer) offers an ideal composition with its combination of melt viscosity, thermal stability, and high char yield after carbonization (discussed later). Any B-Pitch/Pitch blended precursors with <30 wt.% isotropic pitch will require special melt-processing equipment in their production.

Thermal conversion of B-pitch/pitch blended precursor to CBx material

Figure 5 shows TGA curves for all four melt-processible B-Pitch/Pitch precursors and compares them with both mesophase B-Pitch and the starting isotropic pitch (Table 1). The C-yield of mesophase B-Pitch is 90% at 1000°C, while the isotropic pitch only offers a 57% C-yield. All four B-pitch precursors showed C-yields between 57% and 90%. Both melt-processible B-Pitch/Pitch blended precursors 3 and 4 delivered greater than 80% C-yield, significantly higher than those (60-65%) of traditional phenolic resins widely used in C/C manufacturing [50-53]. Overall, the general trend is clear; the higher the B content is, the higher the C-yield. In detail, the onset of weight loss was also delayed from 250°C for isotropic pitch to 350°C for all B-Pitch/Pitch blended precursors, and the rate and extent of weight loss were inversely proportional to the B content. Most of the weight loss occurred below 600°C during the thermal-induced transformation of the precursor structure to the initial CB_x structure. Overall, all the experimental

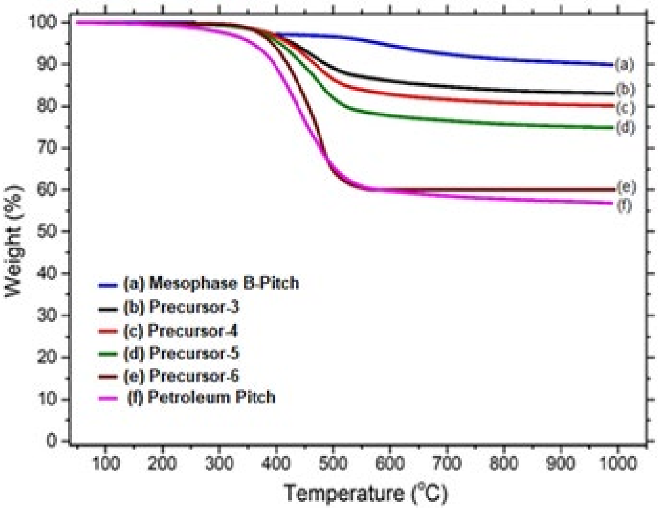

Figure 5. TGA curves of (a) mesophase B-Pitch, (b) precursor-3, (c) precursor-4, (d) precursor-5, (e) precursor-6, and (f) isotropic pitch (heating rate: 10 oC/min) in N2

results imply that the substitutional B elements in the blended B-Pitch/Pitch precursors catalyze the transformation and enhance C-yield.

Solid-state ^{11}B NMR measurements were also taken to monitor the B moiety during the thermal transformation. Figure 6 shows solid-state 11B NMR spectra of precursor-3 and two resulting CB$_x$ products after heating to 600 and 1000°C, respectively. The starting broad chemical shift in precursor-3 moves to higher field with narrower single peaks centered at 0 ppm and -5 ppm after heating to 600 and 1000°C. Evidently, the B-Pitch/Pitch blended precursor (with multiple B moieties) takes on a much more uniform CB$_x$ molecular structure with increasing molecular mass after intermolecular coupling (cycloaddition) reactions. The starting acidic B moieties also gradually increase the electron density (reduce the acidity) via better π-electron conjugation from the enlarged surrounding polycyclic aromatic moieties.

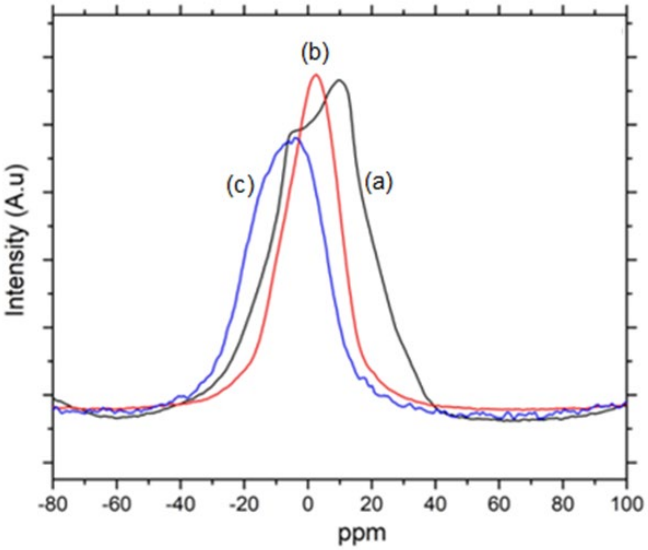

Figure 6. Solid State ^{11}B NMR spectra of Precursor-3 (a) before heating process, and (b) after heating to 600ºC and (c) 1000ºC, respectively

The B-Pitch/Pitch precursor-3 was further heat-treated at higher temperatures, up to 2300°C, under an argon atmosphere. The resulting graphite-like CB$_x$ structures were analyzed by a combination of ICP elemental analysis, Raman spectroscopy, and X-ray diffraction. The B content in the resulting CB$_x$ material after heat treatment at 2300°C decreases to 2.2 wt.% based on ICP elemental analysis, which is consistent with the B solubility limit in a flat graphene sheet with multiple stacking crystallites [22,23]. Figure 7 shows the Raman spectra obtained using a laser excitation wavelength at 514.5 nm (2.41 eV) for several CBx products after thermal conversion under an argon atmosphere at 1000, 1900, 2100, and 2300°C. In addition to an ordered G-band at 1582 cm^{-1} and a disorder-induced D-band at 1350 cm^{-1}, a G'-band at ~2690 cm^{-1} (the overtone of the D-band) is also observed, which becomes sharper and more intense with increasing temperature. Figure 7 (b) shows the integrated intensity ratio (I_D/I_G) of the D and G bands, which is inversely proportional to the carbonization temperature and decreases to 0.31 for CB$_x$ after heating at 2300°C. The I_D/I_G ratio is widely used to quantify the degree of disorder (defects) and is also known to be inversely proportional to the in-plane crystallite sizes (La) [54-56]. The small I_D/I_G=0.31 value indicates that this polycrystalline CB$_x$ material has a high degree of crystallinity and a large crystallite size (La ~62 nm) [56]. The sharp and intense G'-band, which is very sensitive to the stacking order of graphene sheets along the c axis, is quite similar to those of low-defect graphite materials [57].

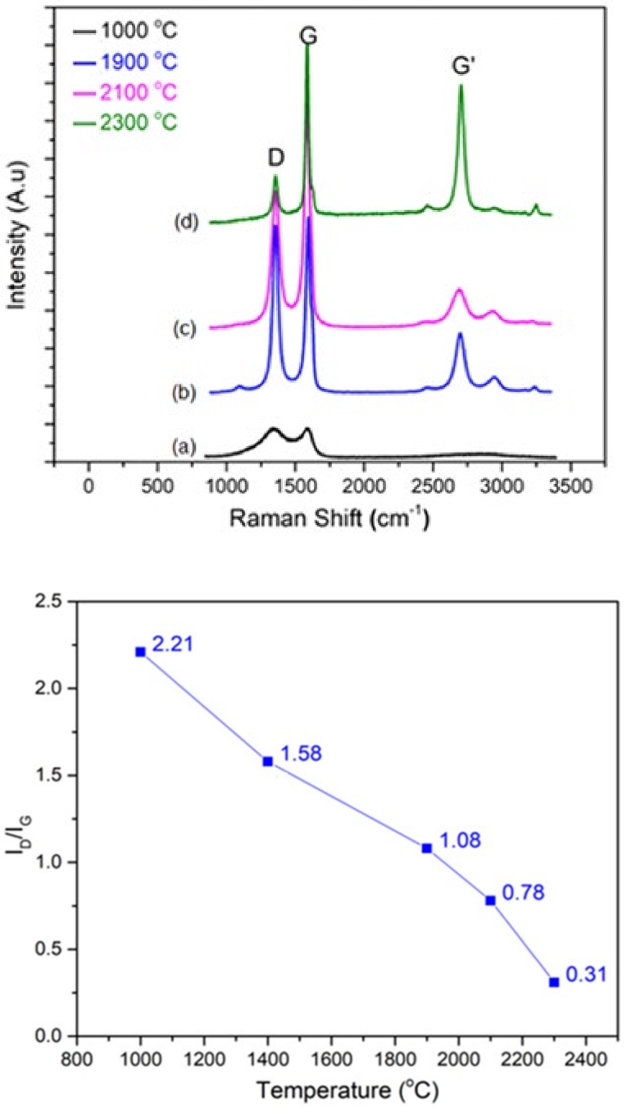

Figure 7. (top) Raman spectra of the resulting CB$_x$ materials after thermal treatment of precursor-3 at (a) 1000, (b) 1900, (c) 2100, and (d) 2300ºC, (bottom) the ratio of the D and G band intensities (I_D/I_G) vs heating temperature

Figure 8 shows the X-ray diffraction (XRD) patterns of several finely ground CB$_x$ powder products prepared from the same precursor-3 at 1000, 1400, 1900, and 2300°C under an argon atmosphere. The two distinctive

X-ray peaks at 2θ~24 (002) and ~43 (100) are typical of graphene crystallites that start to appear at ~1000°C and grow with an increase in temperature [58]. After the temperature reaches 2300°C, the (002) peak becomes very sharp and intense, accompanied by some secondary (101) and (004) peaks. The crystallite parameters, including crystallite stacking height (Lc) and d-spacing, were calculated from the (002) peak using the Scherrer equation and Bragg's law, respectively [59]. Figure 9 compares the interlayer d-spacing (d002) and the stacking height (Lc) between CBx materials and the corresponding C materials prepared from petroleum pitch precursor under the same thermal-treatment conditions.

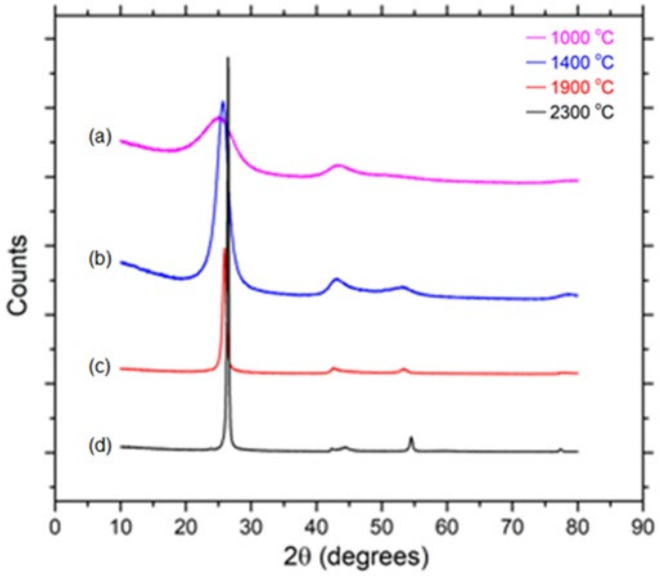

Figure 8. X-ray diffraction pattern of the resulting CB_x material after thermal conversion at (a) 1000, (b) 1400, (c) 1900, and (d) 2300°C

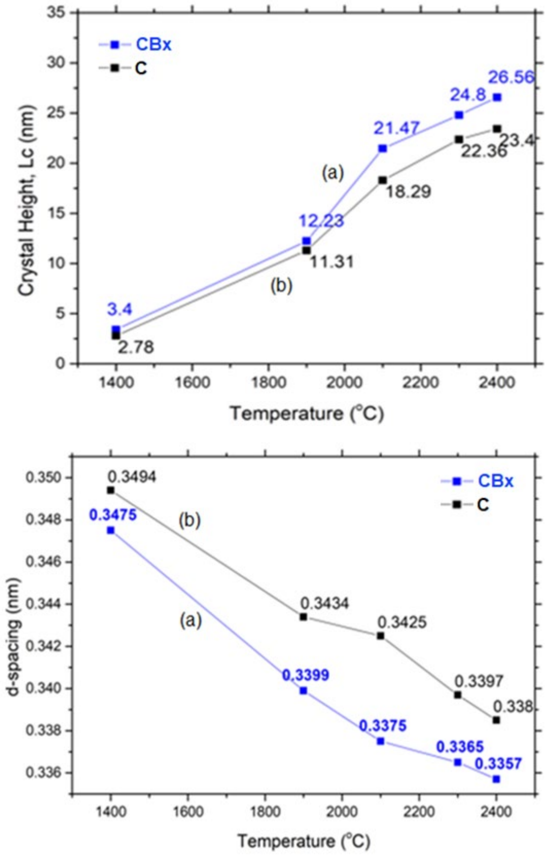

Figure 9. Comparison of (top) crystal height and (bottom) d-spacing between (a) CB_x and (b) C products after thermal conversion under various temperatures from precursor-3 and petroleum pitch precursor, respectively

Similar to the crystal width (La) estimated by the Raman spectrum, the crystal height (Lc) from the XRD pattern also shows an enlarged crystal size with increasing heat treatment temperature, while the interlayer d-spacing decreases proportionally. Compared with the corresponding C materials prepared from the starting petroleum pitch precursor, the consistently smaller d-spacing and larger La and Lc values in the CB_x clearly indicate that the boron catalyzes in situ carbonization/graphitization to form a CB_x product with larger crystallite sizes and higher overall crystallinity. It is very interesting to note that the d-spacing of the CB_x material reaches 0.3357 nm, similar to that of natural graphite, which typically requires a much higher temperature (>3000°C) and pressure to achieve using traditional precursors [60-62].

Thermal/oxidation stability of CBx compounds

The resulting CB_x materials were subjected to a thermal/oxidative stability study in air under high temperatures, and the surface changes were examined to understand the possible protection mechanism. Figure 10 (top) compares TGA curves between the CB_x material (prepared from precursor-3 at 2300°C) and synthetic graphite with a heating rate of 10°C/min in air. The graphite weight begins to decrease at ~550°C, with the weight loss accelerating after >600°C. On the other hand, the CB_x material delays the degradation temperature by nearly 200°C, with initial weight loss at ~750°C and a sharp weight reduction after 800°C. Evidently, the CB_x material is significantly more resistant to thermal/oxidation degradation. Figure 10 (bottom) shows the TGA curves of the same CB_x sample under constant temperatures at 600, 700, and 800°C in air. All measurements

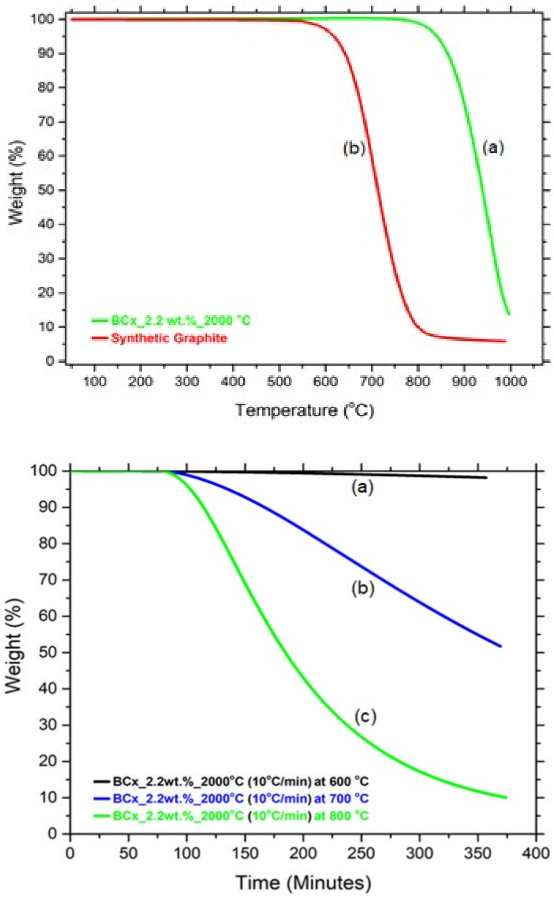

Figure 10. (top) Comparison of TGA curves between (a) CB_x and (b) graphite heated from room temperature to 1000ºC in air, (bottom) Comparison of TGA curves of CB_x sample under constant temperatures at (a) 600, (b) 700, and (c) 800ºC in air

showed a resistance time of approximately 80 minutes without detecting any weight loss. At 600°C in air, the CB_x sample retains 98% of its weight after 6 hours. It then loses approximately 50% of its weight at 700°C and 90% at 800°C.

To comprehend the mechanism by which the CB_x material is protected from thermal/oxidative degradation, the residue that remains after air exposure at 700 and 750°C was analyzed using X-ray photoelectron spectroscopy (XPS). XPS probes the top surface layer (up to 3-6 nm deep) of the samples. Figure 11 shows XPS spectra of B (1s), C (1s), and O (1s) on the CB_x surface and after heating in air at 700°C for 10 min, 1 hr, 3 hrs, and at 750°C for 5 hrs. The surface of the initial CB_x sample shows primarily C elements, and the 2% B content in the CB_x was undetectable. During the time sweep at 700°C in air, both B and O gradually appear on the surface, while the intensity of C starts to decrease. Both B and O surface concentrations continually increase throughout the whole 3-hour heating period. It is very interesting to note that a significant amount of B and O elements were present on the surface after 1 hour of exposure to air at 700°C, despite the fact that the CB_x sample did not show detectable weight loss (based on the kinetic study shown in Figure 10, bottom), and the concentration of C remained high. Even after further exposure to 750°C for 5 hours, C was still detectable on the CB_x surface. It is very likely that a very thin layer of protecting B_2O_3 layer was quickly formed after exposing CB_x to high temperature in air, which reduces oxygen diffusion into the matrix. At 600°C, this thin B_2O_3 surface layer seems very effective in protecting the CBx structure. At 700°C, the B_2O_3 layer very slowly expands into the matrix; only after 80 minutes does the weight loss of the CB_x sample become detectable with a slow progression rate. At 800°C in air, the CB_x material can still maintain its structural integrity for >1 hour (Figure 10, bottom). It is interesting to note that in addition to B_2O_3 species, we also observed boron carbides and a mixture between the two compounds in a high resolution XPS spectrum (Figures S6 and S7 in the Supplemental Information). The experimental results are consistent with the observations made by Jones and Thrower [21], who used FTIR to detect B-O stretch functionalities after exposing the B-doped carbon fiber to oxygen at high temperatures. A summary table (Table S1) of the elemental analysis is also provided in the Supplementary Information with the B, O, and C contents in the oxidized CB_x material.

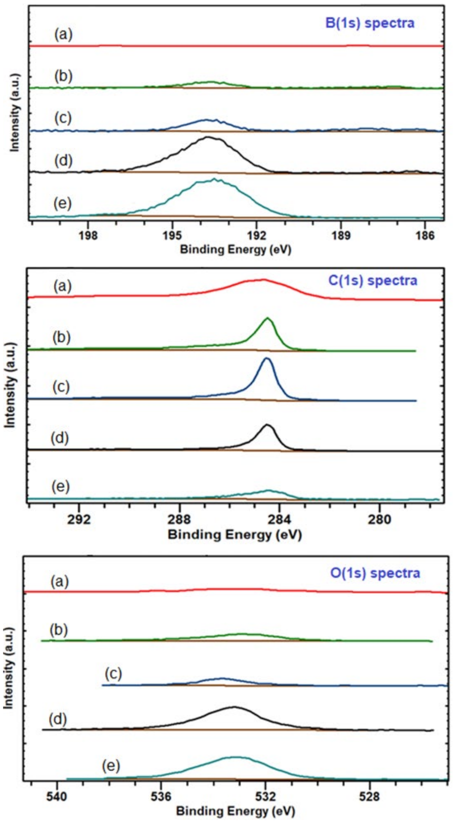

Figure 11. XPS spectra of (top) B(1s), (middle) C(1s), and (bottom) O(1s) on (a) CB_x surface and after heating at 700ºC in air for (b) 10 min, (c) 1 hr, (d) 3 hrs, and (e) at 750ºC for 5 hrs

Conclusion

In this paper, we discuss three closely related objectives, including the preparation of melt-processible B-Pitch/Pitch blended precursors, thermal transformation of these blended precursors to CB_x materials with high C-yields and highly graphitic structures, and the evaluation of the thermal/oxidative stability of the CB_x products. The major goal is to develop a new precursor technology for C/C manufacturing, focusing on reducing the pyrolysis cycles required by increasing char yield and the thermal/oxidative stability of C/C products via the in situ presence of substitutional B elements. Evidently, we have developed a facile, two-step melt-blending route between a borane reagent (DPB) and petroleum pitch to form a melt-processible B-Pitch/Pitch precursor that can be thermally transformed to a CB_x product with ~80% C-yield and a highly graphitic structure with an interlayer d-spacing of 0.3357 nm, similar to that of natural graphite. The resulting CB_x with 2.2 wt.% substitutional B, exhibits excellent thermal/oxidative stability with only 2% weight loss at 600°C in air for 6 hours, as well as a long inhabiting period of 80 minutes at 700 and 800°C in air before detecting weight loss. Apparently, a thin protective B_2O_3 layer was quickly and constantly in situ formed under high temperature in air, which reduced the kinetics of oxygen diffusion into the matrix.

Acknowledgments

The authors would like to thank the US Department of Energy for the financial support through grant DE-EE0008096. The authors would also like to thank Dr. Chenggang Chen and Mr. Brian Rice at the University of Dayton Research Institute for the evaluation of this new precursor technology in the C/C manufacturing.

Conflict Interest

The authors declare that they have no known competing financial interests or personal relationships that could have appeared to influence the work reported in this paper

References

1. McKee, DW. “Oxidation behavior of matrix-inhibited carbon/carbon composites.” *Carbon* 26(1988): 659–64.
2. Westwood, ME, JD Webster, RJ Day and FH Hayes, et al. Oxidation protection for carbon fiber composites.” *J. Mater. Sci* 31(1996): 1389–97.
3. McKee, DW, CL Spiro and EJ Lamby. “The effects of boron additives on the oxidation behavior of carbons.” *Carbon* 22(1984): 507–11.
4. Armitage, P, JR Ebdon, BJ Hunt and MS Jones, et al. “Chemical modification of polymers to improve flame retardance - i. the influence of boron-containing groups.” *Polym. Degrad. Stab* 54(1996): 387–93.
5. Agrawal, A, H Yinnon, DR Uhlmann and RT Pepper, et al. “Boron modification of carbon fibres.” *J. Mater. Sci* 21(1986): 3455–66.
6. Long-gui, T. “Influence of boron treatment on oxidation of carbon fiber in air.” *J. Appl. Polym. Sci* 59(1996): 915–21.
7. Hu, R and TC Chung. “Poly (Acrylonitrile-Co-Vinylcatecholborane): A new precursor for carbon containing B/C, B/N and B/O species.” *Carbon* 34(1996): 595–600.
8. McKee, DW. “Borate treatment of carbon fibers and carbon/carbon composites for improved oxidation resistance.” *Carbon* 24(1986): 737–41.

9. Sheehan, JE. “Oxidation protection for carbon fiber composites.” *Carbon* 27(1989): 709–15.

10. Heh-Won, Chang and MR Robert. “Oxidation behavior of carbon-carbon composites.” *Carbon* 17(1979): 407–10.

11. Wen Fa, Z, L Chun Ling, Y Yong Gang and D Wen Sheng. “The preparation and characterization of boron-containing phenolic fibers.” *Mater. Chem. Phys* 121(2010): 89–94.

12. Zhao, J, Z Xiaohua, L Xiangyi and C Zhengwei, et al. “Accelerating the oxidative stabilization of pitch fibers and improving the physical performance of carbon fibers by modifying naphthalene-based mesophase pitch with c9 resin.” *J Anal Appl Pyrolysis* 154(2021): 105009.

13. Morimoto, T, Y Ogura, M Kondo and T Ueda. “Multilayer coating for carbon-carbon composites.” *Carbon* 33(1995): 351–57.

14. Jin, X, F Xueling, L Chunsheng and T Wang. “Advances in oxidation and ablation resistance of high and ultra-high temperature ceramics modified or coated carbon/carbon composites.” *J. Eur. Ceram. Soc* 38(2018): 1–28.

15. Hu, D, F Qiangang, L Bing and L Zhou, et al. “Multi-layered structural designs of mosi2/mullite anti-oxidation coating for sic-coated c/c composites.” *Surf. Coat. Technol* 409(2021): 126901.

16. Snell, L, A Nelson and P Molian. “A novel laser technique for oxidation-resistant coating of carbon-carbon composite.” *Carbon* 39(2001): 991–999.

17. Cairo, CAA, MLA Graça, CRM. Silva and JC Bressiani. “Functionally gradient ceramic coating for carbon-carbon antioxidation protection.” *J. Eur. Ceram. Soc* 21(2001): 325–29.

18. Strife, JR and JE Sheehan. “Protective coatings for carbon-carbon composites.” *Surf. Eng* 5(2018): 887–91.

19. Aoki, K, MY Cheng, T Hirai and S Yajima. “Thermal expansion of siliconated pyrolytic carbon.” *J. Mater. Sci* 9(1974): 1159–64.

20. Xiaofei, Z, Y Zhang, S Yangyang and F Yanqin, et al. “SiC-Si coating with micro-pores to protect carbon/carbon composites against oxidation.” *J. Eur. Ceram. Soc* 41(2021): 114–120.

21. Jones, LE and PA Thrower. “Influence of boron on carbon fiber microstructure, physical properties and oxidation behavior.” *Carbon* 29(1991): 251–69.

22. Lowell, CE. “Solid solution of boron in graphite.” *J. Am. Ceram. Soc* 50(1967): 142–44.

23. Turnbull, JA, MS Stagg and WT Eeles. “Annealing studies of boron-doped graphite by electron microscopy and X-ray diffraction.” *Carbon* 3(1966): 387–92.

24. Endo, M, C Kim, T Karaki and T Tamaki, et al. “Structural analysis of the b-doped mesophase pitch-based graphite fibers by raman spectroscopy.” *Phys. Rev. B Condens. Matter* 58(1998): 8991–96.

25. Kalijadis, A, Z Jovanović, M Laušević and Z Laušević. “The effect of boron incorporation on the structure and properties of glassy carbon.” *Carbon* 49(2011): 2671–78.

26. Burgess, JS, CK Acharya, J Lizarazo and N Yancey, et al. “Boron-doped carbon powders formed at 1000°c and one atmosphere.” *Carbon* 46 (2008): 1711–17.

27. Xianxian, W and LR Radovic. “Inhibition of catalytic oxidation of carbon/carbon composites by boron-doping.” *Carbon* 43(2005): 1768–77.

28. Young Jae, L and LR Radovic. “Oxidation inhibition effects of phosphorus and boron in different carbon fabrics.” *Carbon* 41(2003): 1987–97.

29. Da-Wei, W, L Feng, ZG Chen and G Qing Lu, et al. “Synthesis and electrochemical property of boron-doped mesoporous carbon in supercapacitor.” *Chem. Mater* 20(2008): 7195–7200.

30. Jens Peter, P and A Thomas. “Doping carbons beyond nitrogen: An overview of advanced heteroatom doped carbons with boron, sulphur and phosphorus for energy applications.” *Energy Environ. Sci* 6(2013): 2839–55.

31. Panchakarla, LS, KS Subrahmanyam, SK Saha and A Govindaraj, et al. “Synthesis, structure, and properties of boron- and nitrogen-doped graphene.” *Adv. Mater* 21(2009): 4726–30.

32. Wang, H, Y Zhou, D Wu and L Liao, et al. “Synthesis of boron-doped graphene monolayers using the sole solid feedstock by chemical vapor deposition.” *Small* 9(2013): 1316–20.

33. Howe, JY and LE Jones. “Influence of boron on structure and oxidation behavior of graphite fiber, P120.” *Carbon* 42(2004): 461–67.

34. Zhai, X, J Liu, Y Zhang and Q Fan, et al. “Microcrystal structure evolution of mesophase pitch-based carbon fibers with enhanced oxidation resistance and tensile strength induced by boron doping.” *Ceram. Int* 45(2019): 11734–38.

35. Raymond, H and TC Chung. “Co-carbonization of 9-chloroborafluorene and pitch; synthesis of B/C materials.” *Carbon* 35(1997): 1101–9.

36. Singleton, DA and L Shun-Wang. “In situ formation of alkenyl- and alkynylboranes for diels-alder reactions by boron-silicon exchange with alkenyl- and alkynylsilanes.” *J Organomet Chem* 544(1997): 157–61.

37. Menetrier, M, T Shirasaki, A Derre and A Tressaud, et al. “Synthesis and characterization of boron-substituted carbons.” *Carbon* 38(2000): 1461–67.

38. Salim, O and TK Mal. “NMR spectroscopy analysis of asphaltenes.” *Energy and Fuels* 33(2019): 10391–414.

39. Zhang, W, JT Andersson, H Joachim-Räder and K Müllen. “Molecular characterization of large polycyclic aromatic hydrocarbons in solid petroleum pitch and coal tar pitch by high resolution MALDI ToF MS and insights from ion mobility separation.” *Carbon* 95(2015): 672–80.

40. Dickinson, EM. “structural comparison of petroleum fractions using proton and 13C n.m.r. spectroscopy.” *Fuel* 59(1980): 290–94.

41. Brooks, JD and GH Taylor. “The formation of graphitizing carbons from the liquid phase.” *carbon* 3(1965): 185-193.

42. Hidemasa, H. “Carbonaceous mesophase: history and prospects.” *Carbon* 26(1988): 139–56.

43. Bermudez, V, S Lukubira and AA Ogale. “Pitch precursor-based carbon fibers.” C*omprehensive Composite Materials* (II) 1(2018): 41-65.

44. Liu, HC, AT Chien, BA Newcomb, Y Liu and S Kumar. “Processing, structure and properties of lignin and cnt incorporated pan based carbon fibers.” *ACS Sustain. Chem. Eng* 3(2015):1943-1954.

45. Hunt, MA, T Saito, RH Brown, AS Kumbhar and AK Naskar. “Carbon fibers: patterned functional carbon fibers from polyethylene.” *Advanced Materials* 24(2012): 2386-2389.

46. Edie, DD and MG Dunham. “Melt spinning pitch-based carbon fibers.” *Carbon* 27(1989): 647–55.

47. Mochida, I, Y Korai, K Cha-Hun and F Watanabe, et al. “Chemistry of synthesis, structure, preparation and application of aromatic-derived mesophase pitch.” *Carbon* 38(2000): 305–28.

48. Fleurot, O and DD Edie. “Steady and transient rheological behavior of mesophase pitches.” *J Rheol (N Y N Y)* 42(1998): 781–93.

49. Collett, GW and B Rand. “Rheological investigation of coal-tar pitches during its transformation to mesophase.” *Fuel* 57(1978): 162–70.

50. Abali, F, K Shivakumar, N Hamidi and R Sadler. “An RTM densification method of manufacturing carbon-carbon composites using primaset PT-30 resin.” *Carbon* 41(2003): 893–901.

51. Pilato, L. “Phenolic resins: a century of progress.” *Springer* 11(2010).

52. Reghunadhan, CP, RL Bindu and KN Ninan. “Thermal characteristics of propargyl ether phenolic resins.” *J. Macromol. Sci. - Pure Appl. Chem* 40 A(2003): 357–69.

53. Learmonth, GS and DP Searle. “Thermal degradation of phenolic resins. v.” *J. Appl. Polym. Sci* 13(1969): 437–43.

54. Tuinstra, F and JL Koenig. “Characterization of graphite fiber surfaces with raman spectroscopy.” *J Compos Mater* 4(1970): 492–99.

55. Tunistra, F and JL Koenig. “Raman spectrum of graphite.” *J. Chem. Phys* 53(1970): 1126–30.

56. Cançado, LG, K Takai, T Enoki and M Endo, et al. "General equation for the determination of the crystallite size l a of nano graphite by raman spectroscopy." *Appl. Phys. Lett* 88(2006): 163106.

57. Xiao, Li, L Haiyan, F Yongjin and ML Sushko, et al. “Low-defect and low-

porosity hard carbon with high coulombic efficiency and high capacity for practical sodium ion battery anode." *Adv. Energy Mater* 8(2018).

58. Kercher, AK and DC Nagle. "Microstructural evolution during charcoal carbonization by x-ray diffraction analysis." *Carbon* 41(2003): 15–27.
59. Warren, BE. "X-Ray diffraction in random layer lattices." P*hys. Rev* 59(1941): 693–98.
60. Xiao, L, L Haiyan, F Yongjin and ML Sushko, et al. "Low-defect and low-porosity hard carbon with high coulombic efficiency and high capacity for practical sodium ion battery anode." *Adv. Energy Mate*r 8(2018).
61. Kercher, AK and DC Nagle. "Microstructural evolution during charcoal carbonization by x-ray diffraction analysis." *Carbon* 41(2003): 15–27.
62. Warren, BE. "X-Ray diffraction in random layer lattices." *Phys. Rev* 59(1941): 693–98.

How to cite this article: Joseph, VS, Wei Z, Houxiang L and TC Mike Chung*. "Developing a Practical Chemical Process to Prepare Boron-Doped Carbon (CB_x) Materials with High Thermal-Oxidative Stability." *J Material Sci Eng* 10 (2021): 1-9